

Class-Dependent Hybrid Data Augmentation for Multiclass Migraine Classification under Severe Class Imbalance

Elvin Somón Sánchez*, Miguel A. Gutiérrez-Naranjo

*Department of Computer Science and Artificial Intelligence
University of Seville, Seville, Spain,*

Abstract

Background and Objective: Multiclass migraine classification from clinical data is hindered by severe class imbalance, limited sample sizes, and methodological biases such as data leakage and inappropriate evaluation metrics, while the impact of data augmentation design remains insufficiently understood. This study investigates how augmentation strategies affect model reliability and proposes a class-dependent framework for imbalanced clinical classification.

Methods: We conducted a reproducibility-oriented reevaluation of prior migraine classification studies, correcting for data leakage and metric bias, and introduced (i) a clinically motivated aggregation of two hemiplegic subtypes following ICHD-3 §1.2.3, (ii) a class-dependent hybrid augmentation strategy that assigns generators by per-class sample size, and (iii) the concept of *fidelity asymmetry*, motivating proportionally constrained growth as an alternative to full class balance. Experiments used 400 patients across seven subtypes under a two-stage protocol, evaluated with stratified 5-fold cross-validation and macro-averaged F1.

Results: Correcting these flaws collapsed previously inflated accuracies (up to 99.7% under leakage) onto a leakage-free macro-F1 scale, on which the best prior model reaches only 0.803 (seven classes). Averaged across the eight classifiers, the framework outperformed individual augmenters (0.862 vs.

*Corresponding author.

Email address: elvsomsan@alum.us.es (Elvin Somón Sánchez)

0.836 Copula, 0.815 CTGAN, 0.801 no augmentation), peaking at 0.914 ± 0.047 (FT-Transformer, proportional augmentation). Clinically motivated class aggregation (FT-Transformer, 0.896 ± 0.038) accounts for most of the gain; the framework’s principal contribution is improved average robustness across classifiers.

Conclusions: Augmentation design is a critical and underexplored factor in medical machine learning. Class-dependent and proportionally constrained augmentation improves reliability under severe imbalance, while label design remains the primary determinant of performance.

Keywords: Migraine, Multiclass classification, Machine learning, Class imbalance, Data augmentation, Clinical decision support

1. Introduction

Migraine is one of the most prevalent and disabling neurological disorders worldwide, affecting approximately 14% of the adult population and representing a leading cause of years lived with disability [1]. From a clinical perspective, migraine is a complex neurovascular disorder involving multiple pathophysiological mechanisms, including cortical spreading depression, trigeminovascular activation, and altered sensory processing [2]. These mechanisms contribute to substantial heterogeneity in symptom presentation, disease progression, and treatment response, complicating accurate diagnosis and subtype differentiation in routine clinical practice. This heterogeneity has direct implications for treatment selection and prognosis, making reliable subtype classification a clinically relevant objective. Despite advances in clinical understanding, migraine diagnosis remains challenging due to overlapping symptom profiles across the subtypes defined in ICHD-3, which distinguishes over a dozen migraine variants with partially shared clinical criteria [3].

In this context, machine learning (ML) approaches have been increasingly explored to support automated classification and clinical decision-making. Several studies have reported promising results using clinical, questionnaire-based, and imaging-derived features [4, 5, 6]. However, recent reviews consistently highlight substantial methodological limitations, including poor reproducibility, limited external validation, and frequent deviations from reporting standards [4, 5, 6, 7].

A central challenge in migraine classification is the reliance on small and

highly imbalanced clinical datasets, particularly in multiclass settings where rare but clinically relevant subtypes may be represented by only a few samples [8, 9]. This imbalance reflects real-world clinical registries but introduces significant difficulties for model training, evaluation, and reproducibility [10]. When not properly addressed, models tend to favour majority classes, leading to inflated performance estimates that do not reflect true clinical utility.

This issue is compounded by the use of inadequate evaluation metrics. Accuracy and micro-averaged scores are dominated by majority-class predictions and can obscure poor performance on minority subtypes. In contrast, macro-averaged F1 assigns equal importance to all classes and provides a more reliable assessment under severe imbalance [11, 12]. For this reason, we adopt macro-F1 as the primary evaluation metric, as it better reflects the need for consistent performance across all clinically relevant subtypes.

Beyond class imbalance, an additional and underexplored limitation lies in the design of data augmentation strategies. Classical oversampling methods such as SMOTE, as well as more recent generative approaches, are typically applied uniformly across all classes [13, 14, 15]. However, this uniform treatment ignores subtype-specific data characteristics and may generate implausible samples, amplify dataset biases, and inflate performance estimates. This effect compounds the distortion introduced by class imbalance and can lead to overly optimistic conclusions.

In this study, we address these limitations through five interrelated contributions, summarised below and presented in detail in the remainder of the paper. We conduct a *reproducibility-oriented reevaluation* of prior migraine classification studies [9, 8], quantifying the impact of augmentation design and evaluation protocols on reported performance. On this corrected baseline, we propose a class-dependent hybrid augmentation framework that adaptively assigns augmentation strategies to each subtype based on its sample size, in contrast to conventional uniform augmentation. The framework, summarised in Fig. 1, partitions classes by a sample-size threshold, assigns a generator to each tier, and controls the absolute volume of synthetic data through a discrete growth mode.

The proposed framework is evaluated on a clinical dataset comprising 400 patients described by 22 features across seven migraine subtypes with highly skewed class distributions. Although moderate in size, this dataset reflects the intrinsic imbalance of specialised clinical registries. To ensure robust evaluation, we adopt a two-stage experimental design, considering both the full seven-class setting and a refined six-class configuration in which the two

hemiplegic migraine subtypes (sporadic and familial), clinically defined by ICHD-3 §1.2.3 as variants of the same syndrome, are merged into a single class. The clinical and statistical rationale for this aggregation is presented in Section 5.2.

The main contributions of this work are:

1. A reproducibility-oriented reevaluation of migraine classification studies, identifying data leakage and reevaluating every prior-art classifier under a leakage-free per-classifier protocol; the strongest prior model reaches only macro-F1 0.803, far below the inflated accuracies originally reported (full per-model results in Appendix A.6).
2. A systematic benchmark of classifiers and augmentation methods under leakage-free stratified 5-fold cross-validation.
3. A clinically and statistically justified aggregation of the two hemiplegic migraine subtypes (sporadic and familial) into a single ICHD-3-grounded category, which addresses the structural performance ceiling observed in the seven-class formulation.
4. A class-dependent hybrid augmentation framework that adapts generation strategies to per-class data characteristics.
5. The introduction of *fidelity asymmetry* and the demonstration that proportional augmentation improves stability in low-data multiclass settings.

The remainder of this paper is structured as follows. Section 2 reviews related work. Section 3 describes the dataset and methods. Section 4 presents the results. Section 5 analyses and discusses the findings, and Section 6 concludes the paper.

2. Related Work

2.1. Machine Learning for Migraine Classification

The application of machine learning (ML) to migraine diagnosis and subtype classification has grown substantially in recent years, driven by the increasing availability of clinical, questionnaire-based, and neuroimaging datasets. Early work in this domain primarily relied on classical supervised learning algorithms, including Support Vector Machines (SVM), k-Nearest Neighbors (KNN), Random Forests (RF), and gradient boosting methods, often combined with feature selection techniques and synthetic oversampling to

mitigate class imbalance [8, 9]. More recently, deep learning and transformer-based architectures originally proposed for general-purpose tabular data have been increasingly explored in biomedical applications, including models such as TabNet, SAINT, FT-Transformer, and TabPFN, which aim to capture complex feature interactions and heterogeneous data distributions more effectively than classical methods [16, 17, 18, 19]. A comprehensive survey of deep neural architectures for tabular data by Borisov et al. [20] provides a structured overview of these developments, categorising them according to their treatment of feature interactions, attention mechanisms, and regularisation strategies. Despite their theoretical advantages, large-scale empirical studies suggest that performance gains over well-tuned classical models are often modest, particularly in small-data regimes typical of clinical applications [21, 22].

Reported performance in migraine classification studies is frequently high, though often difficult to interpret in the absence of class-level analysis. Two prior studies using the same clinical dataset [8, 9] report accuracies between 88% and 99.7% under SMOTE-based augmentation, figures that, as we demonstrate in Section 4.1, are substantially inflated by data leakage and the use of majority-dominated metrics.

However, systematic reviews consistently caution that such results must be interpreted with care, as the literature is characterised by substantial methodological heterogeneity, limited reproducibility, and insufficient external validation [4, 5, 6]. These concerns raise fundamental questions regarding the true generalisation performance and clinical utility of existing models. In response, Petrušić et al. [23] recently proposed an explicit recommendation framework for ML studies in headache classification, emphasising rigorous evaluation procedures, imbalance-sensitive metrics, and reproducible reporting as minimum methodological standards. The present work is directly aligned with these recommendations.

2.2. Class Imbalance and Evaluation in Medical ML

Class imbalance is a well-established challenge in supervised learning and is particularly acute in medical applications, where rare but clinically relevant conditions are inherently underrepresented [10]. In multiclass settings, imbalance introduces complex interactions between class frequency, model capacity, and decision boundaries, often leading to biased models that favour majority classes.

The use of accuracy as a primary evaluation metric in such contexts has been widely criticised, as it is dominated by majority-class predictions and may substantially overestimate model effectiveness [24, 25]. Alternative metrics, such as macro-averaged F1, have been recommended as more appropriate for imbalanced multiclass problems, as they assign equal weight to each class regardless of frequency and better reflect performance on minority classes [11, 12, 26].

Despite these recommendations, many studies in migraine classification continue to report accuracy as their main outcome, often without class-level performance analysis. Furthermore, recent work in medical ML has emphasised the importance of rigorous evaluation protocols, including stratified cross-validation, proper separation of training and test data, and adherence to reporting guidelines such as TRIPOD+AI [7], to ensure reproducibility and clinical relevance.

2.3. Data Augmentation for Imbalanced Tabular Data

Data augmentation is one of the most widely adopted strategies to address class imbalance in tabular datasets. Classical oversampling methods, most notably SMOTE [13] and its variants ADASYN [27] and Borderline-SMOTE [28], generate synthetic samples through interpolation between minority instances. While effective in certain binary classification scenarios, these methods were not originally designed for multiclass problems and apply a uniform interpolation mechanism across all classes. A growing body of work has highlighted the limitations of such approaches, particularly in high-dimensional or severely imbalanced settings, including the introduction of noisy or implausible samples, distortion of class boundaries, and degradation of model performance when minority classes are extremely underrepresented [14, 29].

To address these limitations, generative models for tabular data have been proposed. Among statistically grounded approaches, the Gaussian Copula [30] models multivariate dependencies through a parametric copula structure, offering a principled alternative to interpolation. More flexible architectures such as CTGAN and TVAE [15] adapt conditional GANs and variational autoencoders to the mixed numerical–categorical structure of tabular data, and have been shown to generate more realistic synthetic samples in moderate-data regimes. A comprehensive review of tabular synthetic data generation methods by Fonseca and Bacao [31] surveyed over seventy algorithms and concluded that deep generative models better capture com-

plex inter-feature dependencies than interpolation-based approaches, albeit with performance that varies substantially with dataset size and structural complexity. Similarly, Sauber-Cole and Khoshgoftaar [32] provide a focused survey on the use of GANs to alleviate class imbalance in tabular data, documenting both their promise and their sensitivity to training instability in small-sample settings.

Despite these advances, both classical and generative augmentation methods share a fundamental design assumption: they apply a *uniform* augmentation strategy across all classes. This assumption is rarely questioned, yet it ignores the substantial heterogeneity across classes in terms of sample size, feature distribution, and clinical plausibility. In multiclass medical datasets, such heterogeneity is the norm rather than the exception, suggesting that uniform augmentation may be inherently suboptimal. Preliminary observations on the present dataset are consistent with this concern: uniform treatment systematically degrades predictive capacity on minority subtypes, either by introducing implausible synthetic samples (oversampling-based methods) or by failing to capture stable density estimates when per-class sample size falls below the regimes for which deep generative models are designed. These observations motivate a class-dependent augmentation policy in which the choice of generator is informed by per-class sample size and the resulting real-to-synthetic ratio.

2.4. Data Leakage and Experimental Protocols

In addition to model selection and augmentation design, experimental protocol plays a critical role in determining the validity of reported results. Data leakage, defined as the unintended use of information from the test set during model training, has been identified as one of the most common sources of performance inflation in applied machine learning [33, 34].

A particularly frequent form of leakage in imbalanced learning arises when data augmentation is applied prior to train/test splitting, allowing synthetic samples derived from training instances to appear in the evaluation set. This violates the independence assumption underlying standard evaluation protocols and can lead to substantial overestimation of model performance.

Reevaluations of prior work in migraine classification reveal that such issues are not merely theoretical. In the study by Khan et al. [8], SMOTE was applied globally before data partitioning, resulting in artificially inflated accuracy values. When the experimental protocol is corrected by restricting

augmentation to the training folds within stratified cross-validation, performance drops substantially, and discrepancies between accuracy and macro-F1 become evident. These findings are consistent with broader evidence from biomedical ML indicating that leakage and protocol mis-specification are major drivers of irreproducibility [33, 34].

These methodological concerns (majority-dominated metrics, uniform augmentation strategies, and data leakage) are often discussed in isolation in the migraine classification literature. The present study addresses them jointly under a single reproducible protocol, with the aim of providing a more transparent and conservative assessment of model performance in this clinical setting.

3. Methodology

3.1. Problem Definition and Notation

Let $\mathcal{D} = \{(x_i, y_i)\}_{i=1}^N$ denote a tabular clinical dataset, where $x_i \in \mathbb{R}^d$ represents a vector of d features describing a patient, and $y_i \in \mathcal{C} = \{c_1, \dots, c_K\}$ is the corresponding migraine subtype label. The dataset is characterised by strong class imbalance, with class frequencies $n_k = |\{i : y_i = c_k\}|$ spanning more than one order of magnitude.

The goal is to learn a classifier $f : \mathbb{R}^d \rightarrow \mathcal{C}$ that achieves balanced predictive performance across all classes, assigning equal importance to majority and minority subtypes rather than prioritising either. Performance is evaluated using macro-averaged F1-score, defined as the unweighted mean of per-class F1 scores, which operationalises this balanced objective by giving every class the same weight in the overall metric [11, 12].

3.2. Dataset and Experimental Setup

The data used in this study consist of a publicly available migraine classification corpus that has previously been used by Khan et al. [8] and Reddy and Reddy [9]; access details are provided in the Data availability statement at the end of this paper. According to Khan et al., the underlying records were originally collected at the Hospital Materno Infantil de Soledad (Atlántico, Colombia). It comprises $N = 400$ patients described by 22 clinical features after the removal of the *Ataxia* variable (constant across all patients in the public release and therefore non-informative). Each record is annotated with one of seven migraine subtypes defined by the ICHD-3 classification [3], with class sizes ranging from 14 to 247 samples. A second,

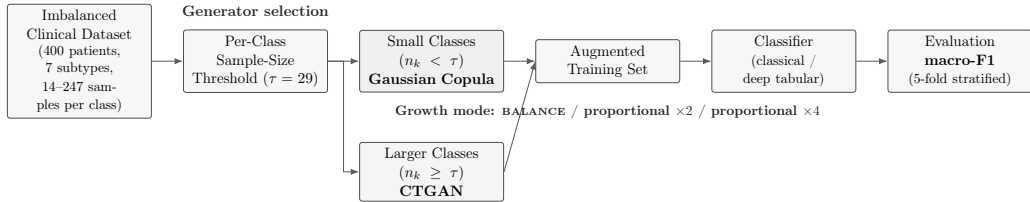


Figure 1: Class-dependent hybrid augmentation framework. The training data are partitioned by class size: classes with fewer than $\tau = 29$ samples are augmented with Gaussian Copula, while larger classes are augmented with CTGAN. The volume of synthetic data is controlled independently by the growth mode (full balance, proportional $\times 2$, or proportional $\times 4$). The resulting augmented training set feeds a classifier whose performance is evaluated under stratified 5-fold cross-validation using macro-averaged F1.

six-class formulation is additionally evaluated, in which the two hemiplegic migraine subtypes (sporadic and familial) are merged into a single ICHD-3-grounded category; the clinical and statistical justification of this aggregation is presented in Section 5.2. Fig. 1 summarises the resulting class-dependent hybrid augmentation framework, which is described in detail in Section 3.5.

3.3. Experimental Protocol and Reproducibility

All experiments are conducted under stratified 5-fold cross-validation, ensuring preservation of class distributions across folds. To prevent data leakage, all preprocessing steps, including data augmentation, are applied exclusively within the training folds.

Hyperparameter selection is performed via grid search across separate experimental runs: for each model, candidate configurations are evaluated under identical fold splits, and the best configuration per model is carried forward to the final benchmark. To avoid conflating distributional shift with suboptimal regularisation, hyperparameters are re-optimised separately for the no-augmentation and augmented regimes, ensuring that augmented and non-augmented configurations are compared at their respective optima. The resulting classifier and augments hyperparameters are listed in Tables A.5 and A.6 (Appendix A.1). Final performance is reported as mean \pm standard deviation across the 5 folds.

Augmentation is performed using SDV [30] for Gaussian Copula and CTGAN, and imbalanced-learn [35] for the SMOTE-family oversamplers. Each augments is fitted independently within each training fold and is required to meet a per-augments minimum sample requirement on every minority

class; configurations that would not satisfy this requirement are reported as failures rather than substituted by an alternative method, preventing silent fallbacks across augmentation strategies. All runs use a fixed random seed of 42. Library versions, runtime configuration and hardware are detailed in Appendix A.2 (Table A.7).

3.4. Exploration of Model and Augmentation Spaces

Before exploring new models, we reproduced every classifier reported in the two prior studies under the leakage-free protocol described above. From Khan et al. [8] we reproduced Support Vector Machine, k-Nearest Neighbors, Decision Tree, Random Forest and a deep neural network; from Reddy and Reddy [9] we reproduced Logistic Regression, Support Vector Machine, Random Forest and an artificial neural network. Reported hyperparameters were respected exactly, and unreported ones followed library defaults (documented per model in Appendix A.6). Evaluated under stratified 5-fold cross-validation with no augmentation, the strongest prior classifier reaches macro-F1 0.803, with a mean of 0.731 across the eight configurations and a range of 0.556 to 0.803; the full per-classifier results, with and without SMOTE, are reported in Table A.12 (Appendix A.6). We adopt the strongest leakage-free prior model as the comparison baseline. Starting from this baseline, we performed a systematic exploration of both the classifier space and the data augmentation space.

3.4.1. Classification Models

The evaluated models include classical machine learning algorithms as Support Vector Machines (SVM), k-Nearest Neighbors (KNN), Random Forest (RF), XGBoost and deep learning architectures specifically designed for tabular data.

The latter span four architectural families with distinct inductive biases:

- **MLP**: a feedforward fully connected network applied directly to the standardised feature vector, without any inter-feature interaction module beyond the linear layers.
- **TabNet** [16]: a sequential architecture that applies sparse attention masks at each decision step to perform instance-wise feature selection, combining the masks with an additive aggregation of step outputs.

- **FT-Transformer** [18]: tokenises each numerical and categorical feature into a learned embedding and processes the resulting sequence with multi-head self-attention transformer blocks, enabling explicit modelling of pairwise feature interactions.
- **GANDALF** [36]: stacks Gated Feature Learning Units (GFLU) that apply learnable sparse gating to feature representations; rather than computing attention weights over a sequence, GFLU implements a multiplicative selection mechanism over individual features.

Both classical and deep models are included to provide a comprehensive benchmark across architectural families. The MLP serves as a deep tabular baseline against which the architectural innovations of the remaining three models (sparse step-wise attention, full self-attention, gated feature units) can be measured.

3.4.2. Data Augmentation Techniques

We evaluated augmentation techniques spanning three main families:

(i) *Oversampling-based methods.* SMOTE and its variants (including Borderline-SMOTE, ADASYN, SVM-SMOTE, SMOTE-ENN and SMOTE-Tomek) generate synthetic samples through interpolation between minority-class instances. SMOTE-ENN and SMOTE-Tomek further combine SMOTE oversampling with edge-cleaning rules (Edited Nearest Neighbors and Tomek-link removal, respectively) aimed at reducing the boundary noise introduced by interpolation [13, 27, 28, 35].

(ii) *Probabilistic joint-distribution models.* Gaussian Copula [30] fits a parametric copula structure to the joint distribution of features, providing a principled alternative to interpolation that remains stable in low-sample regimes.

(iii) *Deep generative models.* CTGAN and TVAE [15] adapt conditional GANs and variational autoencoders to the mixed numerical–categorical structure of tabular data, aiming to capture non-linear feature dependencies when sufficient data are available to fit their adversarial or variational training objectives.

3.5. Class-Dependent Hybrid Augmentation Framework

3.5.1. Motivation

During preliminary experimentation, we observed that different augmentation methods exhibit heterogeneous performance across classes. In particular, generative models perform better for moderately sized classes, while probabilistic models are more stable in extremely low-sample regimes.

This observation suggests that the common practice of applying a uniform augmentation strategy across all classes is suboptimal.

3.5.2. Framework Definition

We define a class-dependent augmentation policy as a mapping:

$$\mathcal{A} : \mathcal{C} \rightarrow \mathcal{M}$$

where \mathcal{M} is the set of available augmentation methods.

For each class c_k , the selected augmentation method $\mathcal{A}(c_k)$ depends on class-specific characteristics, including sample size n_k and feature distribution \mathcal{D}_k . Formally, we treat \mathcal{A} as a policy that, for each class c_k , selects the generator that best preserves the per-class joint feature distribution while remaining trainable at the available sample size n_k . In practice, we approximate this selection through a rule-based partition with a single sample-size threshold τ , complemented by a discrete *growth mode* that controls the absolute volume of synthetic data per class. The growth mode is treated as a configuration parameter rather than as part of the policy itself.

3.5.3. Augmentation Policy

The proposed framework defines two complementary decisions: (i) which generator $\mathcal{A}(c_k)$ to use per class, and (ii) how much synthetic data to generate.

Generator selection (\mathcal{A}). A single sample-size threshold τ partitions classes into two regimes:

- For small classes ($n_k < \tau$): Gaussian Copula, which fits a parametric joint distribution that remains stable in low-sample regimes.
- For larger classes ($n_k \geq \tau$): CTGAN, which captures non-linear feature dependencies when sufficient data are available to fit its adversarial training.

The threshold is fixed at $\tau = 29$ in our experiments, motivated by two convergent considerations. Xu et al. [15] explicitly identify imbalanced categorical columns as a source of severe mode collapse in CTGAN, observing that “imbalanced data also leads to insufficient training opportunities for minor classes” and that “if the training data are randomly sampled during training, the rows that fall into the minor category will not be sufficiently represented, thus the generator may not be trained correctly”. Consistent with this design constraint, our preliminary runs on this dataset showed CTGAN training instability for classes with $n_k < 29$ (loss divergence and degenerate per-class output distributions), whereas Gaussian Copula remained stable across the same range.

Volume control (growth mode). Three growth modes are evaluated, all preserving the per-class generator assignment defined above:

- **BALANCE:** each minority class is augmented up to the size of the majority class, achieving full class balance.
- **PROPORTIONAL $\times 2$ and PROPORTIONAL $\times 4$:** every class is multiplied by a constant factor, preserving the original class proportions while uniformly increasing the absolute volume.

The proportional modes are introduced as a means of mitigating fidelity asymmetry, a phenomenon described in Section 5.4. The choice of growth mode is treated as a configuration parameter selected per model based on training-fold performance, and the empirical comparison of the three modes is presented in Section 4.3.

The class-dependent policy and the chosen growth mode are applied independently within each training fold, so that no synthetic sample derived from training data ever leaks into the corresponding validation fold. Software implementation and library versions are documented in Appendix A.2.

4. Results

4.1. Systematic Exploration of Models and Augmentation Techniques

Starting from the leakage-free prior-art baseline, whose strongest classifier reaches macro-F1 0.803 (the deep neural network of Khan et al., see Appendix A.6), we conducted a systematic experimental exploration over the

eight classifiers and nine augmenters (plus a no-augmentation baseline) described in Section 3, covering classical machine learning, deep tabular models and three augmentation families (SMOTE-based oversampling, GAN/VAE-based generative models and parametric joint-distribution approaches).

Consistent patterns emerged across models. CTGAN and Gaussian Copula produced systematic performance gains for several classifiers, including RF, MLP, and TabNet. In contrast, SMOTE and its variants degraded performance for most classifiers in this severely imbalanced multiclass setting, consistent with known limitations of interpolation-based oversampling when class boundaries are non-linear or heavily overlapping [37].

After systematic hyperparameter tuning, the best result in the original seven-class configuration was obtained by FT-Transformer without augmentation (macro-F1 = 0.845 ± 0.029) under stratified 5-fold cross-validation; the complete grid of all eight classifiers against the ten augmentation conditions is reported in Tables A.8 and A.9 (Appendix A.3). FT-Transformer thus improves on the best leakage-free prior model (0.803) by +0.042 in the seven-class setting. Across the entire seven-class benchmark, FT-Transformer without augmentation is the only configuration to reach 0.845, and no other model–augmentation combination exceeds 0.82 (GANDALF without augmentation, 0.817). This concentration of performance just below 0.85, despite extensive variation in both classifier and augmentation strategy, points to a structural ceiling attributable to label granularity rather than insufficient model capacity, as confirmed by the per-class analysis in the next subsection.

4.2. Results after Clinically Motivated Class Aggregation

Given the ceiling observed in the seven-class setting, the classification task was reformulated into a six-class problem by aggregating two clinically related subtypes (see Section 5.2 for clinical and methodological justification). This reconfiguration produced a substantial and consistent improvement across all evaluated models.

Under the six-class configuration, the FT-Transformer without data augmentation achieved a macro-F1 of 0.896 ± 0.038 , while GANDALF reached 0.883 ± 0.014 under the same cross-validation protocol. These results represent a marked improvement over all configurations evaluated in the original seven-class setting and over the best leakage-free prior model (0.803, a +0.093 gain for FT-Transformer), and demonstrate that label granularity constitutes a more binding constraint on classification performance than augmentation volume in this dataset.

4.3. Class-Dependent Hybrid Augmentation with Proportional Growth

Building on these observations, we evaluated the proposed class-dependent hybrid augmentation framework defined in Section 3. For each class, the generator is assigned according to the sample-size threshold $\tau = 29$ (Gaussian Copula below the threshold, CTGAN above). The volume of synthetic data is then determined by the growth mode: BALANCE augments every minority class to the size of the majority class; PROPORTIONAL $\times 2$ and PROPORTIONAL $\times 4$ multiply each class by a constant factor while preserving the original class proportions.

The proportional modes are designed to mitigate *fidelity asymmetry* (formalised in Section 5.4): in fully balanced augmentation, minority classes are dominated by synthetic samples, whereas the majority class remains entirely real, exposing classifiers to per-class distributions of unequal quality. Proportional augmentation enforces a uniform fraction of real data across all classes, providing a more homogeneous learning signal. The choice of growth mode is treated as a configuration parameter selected per model based on training-fold performance.

4.4. Final Benchmark and Best Configurations

Table 1 consolidates the final six-class benchmark, comparing the no-augmentation baseline against the two best individual generators (CTGAN, Gaussian Copula) and the class-dependent hybrid framework with the best growth mode selected per classifier.

Table 1: Macro-averaged F1 scores by classifier and augmentation strategy on the six-class configuration. Results are reported as mean \pm standard deviation across stratified 5-fold cross-validation. The best result per classifier is highlighted in bold.

Cls.	No Aug.	CTGAN	G.C.	Hyb. Bal.	Hyb. $\times 2$	Hyb. $\times 4$
SVM	0.766 \pm 0.028	0.814 \pm 0.038	0.823 \pm 0.047	0.832 \pm 0.040	0.819 \pm 0.061	0.827 \pm 0.065
KNN	0.795 \pm 0.077	0.772 \pm 0.050	0.802 \pm 0.059	0.825 \pm 0.043	0.843 \pm 0.067	0.859 \pm 0.046
RF	0.819 \pm 0.059	0.758 \pm 0.013	0.848 \pm 0.021	0.832 \pm 0.064	0.840 \pm 0.073	0.806 \pm 0.061
XGBoost	0.746 \pm 0.048	0.799 \pm 0.020	0.808 \pm 0.057	0.817 \pm 0.062	0.823 \pm 0.050	0.795 \pm 0.056
MLP	0.813 \pm 0.042	0.847 \pm 0.054	0.857 \pm 0.052	0.832 \pm 0.046	0.865 \pm 0.071	0.846 \pm 0.082
TabNet	0.686 \pm 0.071	0.807 \pm 0.062	0.839 \pm 0.048	0.871 \pm 0.043	0.775 \pm 0.072	0.831 \pm 0.077
FTT	0.896 \pm 0.038	0.862 \pm 0.059	0.862 \pm 0.067	0.854 \pm 0.060	0.914 \pm 0.047	0.867 \pm 0.042
GANDALF	0.883 \pm 0.014	0.863 \pm 0.040	0.850 \pm 0.042	0.866 \pm 0.046	0.883 \pm 0.034	0.895 \pm 0.039
Avg.	0.801	0.815	0.836	0.841	0.845	0.841

FTT = FT-Transformer. The hybrid average of 0.862 reported in the Abstract corresponds to the per-classifier maximum across the three hybrid growth modes.

To complement Table 1, Tables 2 and 3 report the complete pivot of all evaluated augmenters against the classical and deep tabular classifiers respectively, including the SMOTE family and TVAE excluded from Table 1 for clarity. The split by classifier family follows the architectural distinction introduced in Section 3 and supports the augmenter-wise comparisons used in Section 5.

Table 2: Macro-F1 (mean \pm standard deviation, stratified 5-fold cross-validation) for the six-class configuration across all evaluated augmenters and the four *classical* classifiers. The rightmost column reports the augmenter-wise average across the four classical classifiers; the bottom row reports the classifier-wise average across augmenters.

Augmenter	SVM	KNN	RF	XGBoost	Avg.
No augmentation	0.766 \pm 0.028	0.795 \pm 0.077	0.819 \pm 0.059	0.746 \pm 0.048	0.782
SMOTE	0.718 \pm 0.009	0.689 \pm 0.076	0.780 \pm 0.044	0.763 \pm 0.048	0.738
Borderline-SMOTE	0.711 \pm 0.022	0.708 \pm 0.054	0.748 \pm 0.035	0.750 \pm 0.026	0.729
ADASYN	0.701 \pm 0.053	0.697 \pm 0.091	0.769 \pm 0.015	0.739 \pm 0.023	0.727
SVM-SMOTE	0.762 \pm 0.057	0.715 \pm 0.056	0.780 \pm 0.033	0.763 \pm 0.054	0.755
SMOTE-ENN	0.661 \pm 0.032	0.619 \pm 0.063	0.726 \pm 0.050	0.712 \pm 0.057	0.680
SMOTE-Tomek	0.681 \pm 0.025	0.687 \pm 0.067	0.767 \pm 0.036	0.754 \pm 0.046	0.722
TVAE	0.716 \pm 0.046	0.733 \pm 0.036	0.766 \pm 0.041	0.777 \pm 0.050	0.748
CTGAN	0.814 \pm 0.038	0.772 \pm 0.050	0.758 \pm 0.013	0.799 \pm 0.020	0.786
Gaussian Copula	0.823 \pm 0.047	0.802 \pm 0.059	0.848 \pm 0.021	0.808 \pm 0.057	0.820
Classifier avg.	0.735	0.722	0.776	0.761	—

The hybrid strategy achieves a higher global average performance (macro-F1 = 0.862) than no augmentation (0.801), pure CTGAN (0.815), and pure Gaussian Copula (0.836), outperforming individual augmenters in seven of the eight evaluated classifiers. The single exception is Random Forest, where Gaussian Copula (0.848) slightly exceeds the best hybrid configuration (0.840); the difference falls well within the per-fold standard deviation, consistent with the known sensitivity of bagged tree ensembles to small distributional shifts in the training set.

Best validated configuration. The strongest result observed across the benchmark is FT-Transformer under the proportional $\times 2$ growth mode, reaching macro-F1 = 0.914 \pm 0.047, a +0.111 gain over the best leakage-free prior model (0.803). The closest non-attention configuration is GANDALF under proportional $\times 4$, with macro-F1 = 0.895 \pm 0.039, a +0.012 improvement over its no-augmentation baseline. Both top configurations use the re-optimised hyperparameters listed in Table A.5 (Appendix A.1), tailored to the augmented regime.

Table 3: Macro-F1 (mean \pm standard deviation, stratified 5-fold cross-validation) for the six-class configuration across all evaluated augmenters and the four *deep tabular* classifiers. The rightmost column reports the augmenter-wise average across the four deep classifiers; the bottom row reports the classifier-wise average across augmenters. Abbreviation: FTT \equiv FT-Transformer.

Augmenter	MLP	TabNet	FTT	GANDALF	Avg.
No augmentation	0.813 \pm 0.042	0.686 \pm 0.071	0.896 \pm 0.038	0.883 \pm 0.014	0.820
SMOTE	0.727 \pm 0.071	0.737 \pm 0.043	0.774 \pm 0.052	0.760 \pm 0.063	0.750
Borderline-SMOTE	0.751 \pm 0.100	0.720 \pm 0.065	0.788 \pm 0.030	0.767 \pm 0.037	0.757
ADASYN	0.747 \pm 0.074	0.715 \pm 0.065	0.796 \pm 0.053	0.748 \pm 0.065	0.752
SVM-SMOTE	0.766 \pm 0.060	0.708 \pm 0.029	0.830 \pm 0.039	0.791 \pm 0.009	0.774
SMOTE-ENN	0.672 \pm 0.094	0.637 \pm 0.061	0.711 \pm 0.050	0.690 \pm 0.023	0.678
SMOTE-Tomek	0.670 \pm 0.080	0.731 \pm 0.097	0.766 \pm 0.044	0.750 \pm 0.061	0.729
TVAE	0.743 \pm 0.073	0.709 \pm 0.034	0.813 \pm 0.065	0.795 \pm 0.025	0.765
CTGAN	0.847 \pm 0.054	0.807 \pm 0.062	0.862 \pm 0.059	0.863 \pm 0.040	0.845
Gaussian Copula	0.857 \pm 0.052	0.839 \pm 0.048	0.862 \pm 0.067	0.850 \pm 0.042	0.852
Classifier avg.	0.759	0.729	0.810	0.790	—

Formal pairwise significance testing across folds is left to future work. We note that the observed improvements (e.g., $\Delta = +0.012$ for GANDALF + hybrid $_{\times 4}$, $\Delta = +0.018$ for FT-Transformer + hybrid $_{\times 2}$) are of the same order of magnitude as the per-model fold-level standard deviation (0.038–0.047). Reported gains should therefore be interpreted as point estimates rather than as statistically adjudicated effects, and any claim of “best configuration” carries the inherent variance of a 5-fold evaluation on a 400-sample dataset.

5. Analysis and Discussion

The results presented in Section 4 support three principal claims. First, classifier choice and augmentation family contribute jointly to performance, with neither factor dominating; both must be tuned together rather than studied in isolation. Second, uniform augmentation strategies (and SMOTE-based interpolation in particular) can actively degrade performance in severely imbalanced multiclass settings. Third, label granularity constitutes a more binding constraint on classification performance than augmentation volume, with clinically motivated class aggregation producing larger gains than any augmentation strategy evaluated. The proposed class-dependent hybrid framework, which adapts the generator to per-class sample size and controls volume through a discrete growth mode, outperforms individual augmenters in seven

of the eight evaluated classifiers and provides the best validated configuration of the study. The following subsections analyse the mechanisms underlying each of these findings.

5.1. Performance Ceiling in the Seven-Class Formulation

The persistent performance ceiling observed in the original seven-class formulation was not attributable to insufficient model capacity, lack of hyperparameter tuning, or limited augmentation diversity. Instead, class-wise analysis (Table A.10, Appendix A.4) revealed a pronounced bottleneck driven by two subtypes: *Sporadic Hemiplegic Migraine* (per-class F1 ≈ 0.57) and *Familial Hemiplegic Migraine* (F1 ≈ 0.66), while the remaining five classes achieved a mean per-class F1 of approximately 0.94. This asymmetry constrained the achievable macro-F1, regardless of the classifier or augmentation strategy employed.

5.2. Clinically and Statistically Justified Class Aggregation

This bottleneck reflects an intrinsic limitation of the dataset rather than a modelling failure. According to the ICHD-3 §1.2.3 classification [3], sporadic and familial hemiplegic migraine correspond to subtypes of the same hemiplegic migraine syndrome and share identical symptomatic criteria. The sole diagnostic distinction is the presence of a positive family history, encoded in the dataset by the DPF (*Direct Positive Family history*) variable, a binary indicator of whether the patient has at least one first- or second-degree relative diagnosed with hemiplegic migraine.

While DPF separates the labels, it does not provide discriminative structure for learning the syndrome itself. Quantitative analysis supports this interpretation: of the twenty-two features evaluated, eighteen exhibit absolute mean differences below 0.3 between the two classes, with nine features taking identical constant values in both subtypes (full per-feature breakdown in Table A.11, Appendix A.5). Clustering analysis yields near-zero Silhouette coefficients in opposite directions (+0.123 for sporadic and -0.072 for familial), neither indicating genuine class cohesion. Consequently, the decision boundary separating these labels is weakly supported by the remaining feature space and is largely non-learnable.

Merging both subclasses into a single *Hemiplegic migraine* category is justified from statistical and machine learning perspectives, and is consistent with the symptomatic equivalence established in ICHD-3. However, this aggregation entails a deliberate trade-off: the distinction between familial

and sporadic forms carries clinical relevance for genetic counselling and family screening. The merged classifier therefore cannot replace subtype-specific diagnosis in contexts where this distinction is actionable. Its utility is scoped to settings where the primary objective is syndrome-level identification, and the aggregation should be treated as a dataset-specific modelling decision rather than a general clinical recommendation.

5.3. Why SMOTE-Based Augmentation Degrades Performance

The consistent degradation observed with SMOTE-based augmentation, documented in Section 4.1 and consistent with known limitations in high-imbalance settings [14, 37], is interpretable in terms of the specific geometry of this dataset.

In this dataset, class boundaries are non-linear and partially overlapping, as evidenced by the near-zero Silhouette coefficients reported in Section 5.2. Under these conditions, SMOTE-generated samples from minority classes systematically fall within the feature-space regions of adjacent classes, introducing label noise that degrades macro-F1.

In contrast, distribution-learning approaches such as CTGAN and Gaussian Copula aim to preserve joint feature dependencies and are better aligned with the structure of clinical tabular data, where interactions are often non-linear and non-additive. This effect is particularly pronounced under severe imbalance, where synthetic samples from minority classes may disproportionately contaminate regions of the feature space associated with other classes, ultimately harming macro-F1 [38].

5.4. Fidelity Asymmetry and Proportional Augmentation

Definition. Analysis of fully balanced augmented datasets reveals a structural issue that, to our knowledge, has not been explicitly formalised in the tabular augmentation literature. Although the balanced dataset used in this study is 72.9% synthetic overall, the fraction of real samples is highly class-dependent: the majority class remains entirely real, whereas minority classes contain as little as 7–15% real samples. For the smallest class ($n = 17$), the synthetic-to-real ratio reaches $\approx 13.5:1$. We term this phenomenon *fidelity asymmetry* to distinguish it from the class-frequency imbalance that motivates augmentation.

Mechanism. While class imbalance is addressed by oversampling, fidelity asymmetry is *introduced* by it, representing a second-order effect that is exacerbated by aggressive balancing. This distinction is related to, but distinct from, the concept of synthetic data quality degradation documented in low-sample generative settings [31, 32]: since estimation error is inherent to any generative process, that error is amplified disproportionately for minority classes, and in attention-based architectures that model cross-feature dependencies these discrepancies can destabilise learned representations precisely for the classes that require the greatest discriminative accuracy. From this perspective, augmentation is best treated not as a uniform preprocessing step, but as a model-selection problem over data-generating processes.

Mitigation through proportional augmentation. Proportional augmentation directly addresses fidelity asymmetry by enforcing a uniform fraction of real samples across all classes while preserving the original class proportions. By avoiding forced full balance, this strategy maintains the global structure of the data distribution and provides a more homogeneous learning signal. The gains observed under proportional augmentation (+0.012 macro-F1 for GAN-DALF under $\times 4$ and a peak result of 0.914 ± 0.047 for FT-Transformer under $\times 2$, Table 1) match or exceed those obtained by optimising the augmentation family alone: averaging across the eight classifiers in Tables 2 and 3, the shift from the SMOTE family (~ 0.73) to Gaussian Copula (0.836) yields $\Delta \approx +0.10$, of the same order as the per-classifier gains attributable to growth mode selection. Managing data fidelity is therefore at least as consequential as the choice of generative method, and over-aggressive balancing can be counterproductive in low-data multiclass medical settings.

5.5. Clinical Implications

From a clinical perspective, the proposed framework offers three concrete contributions to migraine subtype classification under realistic data constraints. First, by improving macro-averaged performance on minority subtypes, the approach increases sensitivity to the under-represented diagnoses that are most likely to be missed in routine practice and that carry the highest cost of misclassification, including hemiplegic and basilar-type variants. Second, the explicit separation between label design (clinically motivated aggregation) and learning design (class-dependent augmentation) allows clinicians and methodologists to negotiate trade-offs transparently: a syndrome-level six-class formulation is appropriate for triage and treatment

selection, while a finer seven-class formulation may be retained when family-history information is required for genetic counselling. Third, the leakage-free protocol and per-fold cross-validation design address key methodological concerns highlighted by TRIPOD+AI reporting guidance [7], in particular items related to data partitioning and internal validation; full TRIPOD+AI compliance (including ethical approval, fairness analysis, calibration metrics and open science statements) remains a target for future iterations and is a precondition for integration into clinical decision-support systems. The framework is therefore best understood as an evaluation and data-handling template rather than as a deployable diagnostic tool: external validation on independent cohorts remains the next step before any clinical deployment.

6. Conclusions

This study set out to determine whether the high performance reported in prior migraine classification work reflects genuine predictive capability or methodological artefact. The evidence presented here supports the latter: data leakage, majority-dominated metrics, and uniform augmentation strategies collectively produce inflated estimates that dissolve under rigorous evaluation. Correcting these artefacts reduces previously inflated performance estimates, with the strongest leakage-free prior-art classifier, the deep neural network of Khan et al., reaching macro-F1 0.803 (no augmentation, stratified 5-fold cross-validation, seven-class setting), well below the inflated accuracies of up to 99.7% originally reported. This figure, rather than representing a failure, defines the true starting point from which meaningful improvement is possible.

By performing a reproducibility-oriented reevaluation of prior work, we established this corrected baseline and showed that widely adopted uniform augmentation strategies, particularly SMOTE-based methods, can degrade macro-averaged performance in severely imbalanced multiclass settings. In contrast, generative distribution-learning approaches such as CTGAN and Gaussian Copula proved more robust, especially when combined with classifiers capable of modelling non-linear feature interactions.

A key finding of this work is that apparent performance ceilings may reflect limitations in problem formulation rather than modelling capacity. Through clinically and statistically justified aggregation of hemiplegic migraine subclasses in accordance with the ICHD-3 taxonomy, we removed a non-learnable decision boundary and substantially improved achievable

macro-F1. This result highlights the importance of aligning label structures with underlying clinical entities when designing machine learning tasks in healthcare.

Building on these insights, we proposed and evaluated a class-dependent hybrid augmentation framework that adapts augmentation strategies to class-specific data characteristics. We introduced the concept of *fidelity asymmetry* to explain why fully balanced augmentation can be detrimental in low-data regimes, and showed that proportional augmentation, which preserves class proportions while equalising real-data fractions, offers a more stable and effective alternative.

This work contributes (i) a leakage-free per-classifier reevaluation of every prior-art model (Table A.12, Appendix A.6), establishing the strongest prior model (macro-F1 0.803) as a corrected baseline that re-frames the previously reported performance on this dataset, (ii) a clinically grounded label aggregation derived from ICHD-3 §1.2.3 that resolves the persistent hemiplegic performance ceiling, (iii) a class-dependent hybrid augmentation framework that adapts generation strategies to per-class sample size, and (iv) the formalisation of *fidelity asymmetry* as an underexplored second-order effect of class balancing, together with an empirical demonstration that proportionally constrained growth can match or exceed full balance for most classifiers (Table 1).

The historical progression of results illustrates the cumulative methodological and clinical refinement achieved across this study, from an inflated accuracy of ~ 0.997 under leakage (with macro-F1 unreported) to a rigorous macro-F1 of 0.914 ± 0.047 under the best validated configuration (Table 4). Notably, the largest model-controlled gain attributable to a single decision, from 0.845 to 0.896, was produced not by augmentation but by clinically motivated label redesign, underscoring that problem formulation is the most consequential modelling decision in this dataset.

This study has several limitations that should inform the interpretation of its findings. First, the dataset comprises 400 patients from a single clinical centre, which limits the diversity of clinical phenotypes captured. Second, no external validation cohort is currently available; generalisation of the proposed framework to other clinical sites, populations or migraine taxonomies remains untested and is a precondition for any clinical deployment. Third, the class-dependent augmentation policy relies on a single sample-size threshold (τ) and a choice of growth mode, both selected for the present dataset; their transferability to other class distributions has not been as-

sessed. Fourth, the concept of fidelity asymmetry introduced in Section 5.4, while empirically supported here, lacks a formal theoretical treatment. Fifth, the performance improvement associated with class aggregation depends on the specific non-learnability of the familial, sporadic boundary in this feature set; datasets that include genetic markers or family history encoded with greater resolution may not exhibit the same ceiling. Sixth, the variance of the best-performing configuration (FT-Transformer + hybrid_{×2}, ± 0.047 , see Section 4.4) is larger than the variance of the no-augmentation FT-Transformer baseline (± 0.038) and warrants caution in deployment contexts where predictive stability is as important as mean performance. Finally, all experiments use a fixed random seed (42) for reproducibility, which leaves residual variability attributable to model initialisation and synthetic generation unquantified.

Future work. Several extensions follow naturally from these findings. First, external validation on independent clinical cohorts is required before any clinical deployment. Second, multi-seed averaging would tighten estimates of the variance attributable to model initialisation and synthetic generation, complementing the fixed-seed protocol used here. Third, the concept of fidelity asymmetry warrants formal theoretical treatment, including a characterisation of the conditions under which it dominates other sources of augmentation-induced variance. Fourth, a sensitivity analysis on the threshold τ would clarify the transferability of the class-dependent policy to other class distributions. Finally, formal pairwise statistical testing (Wilcoxon signed-rank with Holm-Bonferroni correction) is recommended to adjudicate the observed deltas against per-fold variance.

Despite these limitations, the findings have broader methodological implications. They suggest that data augmentation should be treated as a context-sensitive design choice rather than a uniform preprocessing step, and that careful alignment between clinical taxonomy, data fidelity, and evaluation protocol is essential for trustworthy medical machine learning. The framework proposed here, by combining leakage-free evaluation, class-dependent augmentation, and proportionally constrained growth, provides a reproducible and clinically grounded template that is directly applicable to any multiclass medical classification problem characterised by low data volume and severe label imbalance.

More broadly, this work suggests that improving medical machine learning systems may depend less on increasingly complex models and more on

rigorous problem formulation, data fidelity, and evaluation design.

CRedit authorship contribution statement

Elvin Somón Sánchez: Conceptualization, Methodology, Software, Investigation, Formal analysis, Data curation, Visualization, Writing – original draft. **Miguel A. Gutiérrez-Naranjo:** Conceptualization, Methodology, Supervision, Writing – review & editing.

Ethics statement

This study analyses a publicly available migraine classification dataset hosted on Kaggle that contains no personally identifiable information. No new patient data were collected for the present work, and no individual identifiers were processed.

Funding

This work was supported by grant CEX2024-001517-M (IMUS, “Apoyo a Unidades de Excelencia María de Maeztu”), funded by MICIU/AEI/10.13039/501100011033. The funding source had no role in the study design; in the collection, analysis and interpretation of data; in the writing of the report; or in the decision to submit the article for publication.

Declaration of competing interest

The authors declare that they have no known competing financial interests or personal relationships that could have appeared to influence the work reported in this paper.

Data availability

The migraine classification dataset analysed in this study is publicly available on Kaggle¹. The same dataset was used in the prior studies by Khan et al. [8] and Reddy and Reddy [9]. No new data were generated for the present work. Experimental configurations, hyperparameter grids and per-fold cross-validation artefacts that support the findings of this study are available from the corresponding author upon reasonable request.

¹<https://www.kaggle.com/datasets/weinoose/migraine-classification>.

Appendix A. Supplementary Tables

This appendix consolidates the implementation details that support the main benchmark, namely (i) the exact hyperparameter configurations used to obtain the macro-F1 values reported in Tables 1, 2 and 3, (ii) the Python libraries and classes underlying each component of the pipeline, (iii) the complete macro-F1 grid for the original seven-class formulation (Appendix A.3), (iv) per-class F1 scores under both label configurations, and (v) the leakage-free reevaluation of every prior-art classifier that defines the comparison baseline (Appendix A.6).

Appendix A.1. Hyperparameter Configurations

Tables A.5 and A.6 report the hyperparameter values applied to each classifier and augmenter in the final benchmark. Classifier hyperparameters were selected via grid search on the six-class configuration as described in Section 3.3; augmenter hyperparameters followed library defaults except where noted.

Appendix A.2. Software Stack and Runtime Environment

All experiments were implemented in Python 3.11 within a dedicated conda environment. Classical models were trained with scikit-learn 1.4; deep tabular models with pytorch-tabular 1.2 over PyTorch 2.10 and PyTorch-Lightning 2.6. Experiments ran on an Apple M1 Max workstation (10-core CPU, 32-core integrated GPU, 32 GB unified memory). Deep tabular models were trained on the integrated GPU through PyTorch’s native MPS backend; classical models on CPU. Table A.7 maps every component of the experimental pipeline to the exact Python class used in the implementation.

Appendix A.3. Complete Seven-Class Benchmark

Tables A.8 and A.9 report the complete macro-F1 grid for the original seven-class formulation, mirroring the six-class pivots of Tables 2 and 3. These results substantiate the performance ceiling discussed in Section 4.1: across all eighty model–augmentation combinations, FT-Transformer without augmentation is the single configuration reaching 0.845, and no other combination exceeds 0.82. The corresponding per-class breakdown in Table A.10 attributes this ceiling to the two hemiplegic subtypes rather than to insufficient model capacity.

Appendix A.4. Per-Class F1 under Both Label Configurations

Table A.10 reports the per-class F1 scores obtained by FT-Transformer (no augmentation) under the seven-class and the six-class formulations, computed as the mean across the five cross-validation folds. The same model is also reported under the proportional $\times 2$ hybrid augmentation in the six-class setting, the configuration that produced the peak macro-F1 of the study (Section 4.4).

Table A.10 shows that all five non-hemiplegic classes already operate near their per-class ceiling under the seven-class formulation; the macro-F1 improvement from 0.845 to 0.896 in the six-class setting is therefore attributable almost entirely to the collapse of the two hemiplegic subtypes into a single, learnable class.

Appendix A.5. Per-Feature Separability between Sporadic and Familial Hemiplegic Migraine

Table A.11 reports, for each of the 22 clinical features (after Ataxia removal), the per-class mean for Sporadic ($n = 14$) and Familial ($n = 24$) Hemiplegic Migraine, together with the absolute difference $|\bar{x}_S - \bar{x}_F|$. The DPF feature is shown for completeness as the only perfect separator (binary family-history indicator). Of the twenty-two features, eighteen exhibit absolute mean differences below 0.3, including nine features that take identical constant values in both subtypes. The remaining four non-trivial separators (Intensity, Sensory, Visual, DPF) account for the residual class signal, of which only DPF is perfectly informative. These figures support the symptomatic equivalence between the two subtypes claimed in Section 5.2.

Appendix A.6. Replication of prior studies classifiers under leakage-free evaluation

To establish an honest comparison baseline, we reproduced every classifier reported by Khan et al. [8] and Reddy and Reddy [9] under the project’s leakage-free protocol: stratified 5-fold cross-validation over the seven ICHD-3 classes, with augmentation (when used) fitted exclusively within each training fold. Reported hyperparameters were respected exactly; unreported ones follow library defaults, documented per model in the note below. Khan et al. name scikit-learn explicitly and describe the deep network in Keras terms, whereas Reddy and Reddy report no software and specify few hyperparameters. The Support Vector Machine (linear, $C = 1$) is common to both papers and is therefore computed once.

Two caveats apply to the comparison. First, the original studies reported *accuracy* (Khan) or classification accuracy / CA (Reddy) obtained *with* pre-split SMOTE, that is, under data leakage, whereas the values in Table A.12 are *macro-F1* obtained *without* leakage; the two sets of figures are therefore not directly comparable. Under leakage, Khan et al. reported accuracies between 88% and 99.7% (with augmentation, SVM 94.60%, KNN 97.10%, Decision Tree 88.20%, Random Forest 88.50%, DNN 99.66%), and Reddy and Reddy reported selective-sampling CA between 0.958 and 0.995 (ANN 0.995, Random Forest 0.980, SVM 0.965, Logistic Regression 0.958). Under the leakage-free protocol the strongest prior model reaches only macro-F1 0.803, with a mean of 0.731 across the eight configurations and a range of 0.556 to 0.803.

Table 4: Macro-F1 attained at successive refinement steps of this study. Each row corresponds to a distinct model–augmentation configuration evaluated independently; values across rows are not additive deltas of a single chain. The largest model-controlled improvement attributable to a single decision is the +0.051 gain from label redesign (FT-Transformer no-augmentation, 7-class \rightarrow 6-class); the augmentation contribution at the peak is +0.018 (FT-Transformer, 6-class, no-aug 0.896 \rightarrow hybrid_{x2} 0.914). Abbreviation: FTT = FT-Transformer.

Refinement step	Configuration	Macro-F1
Original study (with leakage)	DNN + SMOTE applied before split (Khan et al. 99.7% accuracy reported); macro-F1 not reported by the authors	—*
Best prior-art classifier (leakage-free)	DNN (Khan et al.), no augmentation, 7 classes	0.803 ± 0.077
Best classifier (7 classes)	FTT, no augmentation, 7 classes	0.845 ± 0.029
Clinically guided aggregation	FTT, 6 classes, no augmentation	0.896 ± 0.038
Best validated configuration	FTT + hybrid_x2	0.914 ± 0.047

* Macro-F1 was not reported in the original studies (only accuracy). We reproduced all classifiers from both prior studies under a leakage-free protocol (no augmentation, stratified 5-fold): Khan et al. (SVM, KNN, Decision Tree, Random Forest, DNN) and Reddy and Reddy (Logistic Regression, SVM, Random Forest, ANN). The strongest, the DNN of Khan et al., reaches macro-F1 0.803 ± 0.077 (best prior-art classifier, second row), which we use as the honest starting point for subsequent comparisons; the full per-model results appear in Table A.12 (Appendix A.6). The deep tabular architectures introduced in this work (FT-Transformer, GANDALF, TabNet) do not appear in the prior literature and are therefore excluded from this reference baseline.

Table A.5: Final hyperparameters per classifier (six-class benchmark). Deep-tabular models additionally used the default early-stopping configuration of pytorch-tabular 1.2 (monitor: `valid_loss`, patience: 3, `min_delta`: 0.001, mode: `min`) with checkpoint selection on the same metric, and identical fold splits across all models. Abbreviation: FTT = FT-Transformer.

Classifier	Hyperparameters
SVM	<code>C=100, kernel=rbf, gamma=0.1, class_weight=balanced</code>
KNN	<code>n_neighbors=5, weights=uniform, metric=euclidean</code>
Random Forest	<code>n_estimators=300, max_depth=None, class_weight=balanced</code>
XGBoost	<code>n_estimators=300, max_depth=3, learning_rate=0.2</code>
MLP	<code>layers=256-128, dropout=0.2, learning_rate=0.01, batch_size=32, max_epochs=100</code>
TabNet	<code>n_d=32, n_a=32, n_steps=3, gamma=2.0, learning_rate=0.02, batch_size=64, max_epochs=100</code>
FTT	<code>input_embed_dim=128, num_heads=8, num_attn_blocks=2, attn_dropout=0.1, ff_dropout=0.1, learning_rate=5e-4, batch_size=64, max_epochs=150</code>
GANDALF	<code>gflu_stages=10, gflu_dropout=0.01, gflu_feature_init_sparsity=0.1, learning_rate=5e-3, batch_size=64, max_epochs=100</code>

Table A.6: Final hyperparameters per augmenter. SMOTE-family $k_neighbors$ is adapted at runtime to $\min(5, n_{\min} - 1)$ when the smallest class would otherwise violate the neighborhood constraint. Hybrid configurations use the threshold $\tau = 29$ described in Section 3.5.

Augmenter	Hyperparameters
SMOTE	<code>k_neighbors=5</code> (adaptive)
Borderline-SMOTE	<code>k_neighbors=5</code> (adaptive), <code>kind=borderline-1</code>
ADASYN	<code>n_neighbors=5</code> (adaptive)
SVM-SMOTE	<code>k_neighbors=5</code> (adaptive), <code>m_neighbors=10</code>
SMOTE-ENN	SMOTE <code>k_neighbors=5</code> + ENN <code>n_neighbors=3</code>
SMOTE-Tomek	SMOTE <code>k_neighbors=5</code> + Tomek-link cleaning
CTGAN	<code>epochs=300</code> , <code>batch_size=64</code> , <code>pac=1</code> , <code>generator_dim=(128,128)</code> (or <code>(64,64)</code> if $n_k < 30$), <code>discriminator_dim idem</code>
TVAE	<code>epochs=300</code> , <code>batch_size=64</code> , <code>compress_dims=(64,64)</code> , <code>decompress_dims=(64,64)</code>
Gaussian Copula	SDV defaults, <code>min_samples=10</code> preflight check
Hybrid	$\tau = 29$; <code>generator(small)</code> : Gaussian Copula; <code>generator(large)</code> : CTGAN; <code>growth_mode</code> \in {BALANCE, PROPORTIONAL \times 2, PROPORTIONAL \times 4}

Table A.7: Python libraries and classes used for each pipeline component. Library version is reported alongside each entry. Abbreviation: FTT = FT-Transformer.

Component	Library (version)	Class
<i>Classical classifiers</i>		
SVM	scikit-learn 1.4	<code>svm.SVC</code>
KNN	scikit-learn 1.4	<code>neighbors.KNeighborsClassifier</code>
Random Forest	scikit-learn 1.4	<code>ensemble.RandomForestClassifier</code>
XGBoost	xgboost 2.0	<code>XGBClassifier</code>
<i>Deep tabular classifiers (via pytorch-tabular 1.2)</i>		
MLP [‡]	pytorch-tabular 1.2	<code>CategoryEmbeddingModelConfig</code>
TabNet	pytorch-tabular 1.2	<code>TabNetModelConfig</code>
FTT	pytorch-tabular 1.2	<code>FTTransformerConfig</code>
GANDALF	pytorch-tabular 1.2	<code>GANDALFConfig</code>
<i>Oversampling augmenters</i>		
SMOTE	imbalanced-learn 0.12	<code>over_sampling.SMOTE</code>
Borderline-SMOTE	imbalanced-learn 0.12	<code>over_sampling.BorderlineSMOTE</code>
ADASYN	imbalanced-learn 0.12	<code>over_sampling.ADASYN</code>
SVM-SMOTE	imbalanced-learn 0.12	<code>over_sampling.SVMSMOTE</code>
SMOTE-ENN	imbalanced-learn 0.12	<code>combine.SMOTEENN</code>
SMOTE-Tomek	imbalanced-learn 0.12	<code>combine.SMOTETomek</code>
<i>Generative and parametric augmenters (via SDV 1.10)</i>		
CTGAN	SDV 1.10	<code>CTGANSynthesizer</code>
TVAE	SDV 1.10	<code>TVAESynthesizer</code>
Gaussian Copula	SDV 1.10	<code>GaussianCopulaSynthesizer</code>
<i>Cross-validation, metrics, framework</i>		
Stratified k -fold CV	scikit-learn 1.4	<code>model_selection.StratifiedKFold</code>
Macro-F1 metric	scikit-learn 1.4	<code>metrics.f1_score(average='macro')</code>
Deep-model trainer	PyTorch-Lightning 2.6	<code>pytorch.Trainer</code>
Tensor backend	PyTorch 2.10	<code>torch</code>

[‡] The MLP is instantiated through pytorch-tabular’s `CategoryEmbeddingModelConfig`, but with all 22 features configured as continuous (`categorical_cols=[]`). Under this configuration no embedding layer is constructed, and the architecture reduces to a classical multilayer perceptron applied directly to the standardised feature vector.

Table A.8: Macro-F1 (mean \pm standard deviation, stratified 5-fold cross-validation) for the *seven-class* configuration across all evaluated augmenters and the four *classical* classifiers. Layout mirrors Table 2 (six-class). The rightmost column reports the augmenter-wise average across the four classical classifiers; the bottom row reports the classifier-wise average across augmenters.

Augmenter	SVM	KNN	RF	XGBoost	Avg.
No augmentation	0.662 \pm 0.075	0.680 \pm 0.038	0.747 \pm 0.087	0.711 \pm 0.053	0.700
SMOTE	0.597 \pm 0.046	0.627 \pm 0.085	0.730 \pm 0.043	0.711 \pm 0.082	0.666
Borderline-SMOTE	0.601 \pm 0.069	0.639 \pm 0.072	0.703 \pm 0.043	0.695 \pm 0.089	0.659
ADASYN	0.615 \pm 0.071	0.622 \pm 0.075	0.698 \pm 0.061	0.678 \pm 0.087	0.653
SVM-SMOTE	0.610 \pm 0.055	0.605 \pm 0.069	0.720 \pm 0.053	0.693 \pm 0.071	0.657
SMOTE-ENN	0.575 \pm 0.055	0.544 \pm 0.067	0.673 \pm 0.047	0.637 \pm 0.042	0.607
SMOTE-Tomek	0.588 \pm 0.052	0.626 \pm 0.085	0.722 \pm 0.053	0.680 \pm 0.072	0.654
TVAE	0.624 \pm 0.053	0.628 \pm 0.070	0.710 \pm 0.081	0.706 \pm 0.085	0.667
CTGAN	0.744 \pm 0.071	0.688 \pm 0.072	0.756 \pm 0.063	0.768 \pm 0.069	0.739
Gaussian Copula	0.728 \pm 0.091	0.705 \pm 0.082	0.748 \pm 0.062	0.780 \pm 0.063	0.740
Classifier avg.	0.634	0.636	0.721	0.706	—

Table A.9: Macro-F1 (mean \pm standard deviation, stratified 5-fold cross-validation) for the *seven-class* configuration across all evaluated augmenters and the four *deep tabular* classifiers. Layout mirrors Table 3 (six-class). FT-Transformer without augmentation (0.845) is the single highest cell of the entire seven-class grid. Abbreviation: FTT = FT-Transformer.

Augmenter	MLP	TabNet	FTT	GANDALF	Avg.
No augmentation	0.737 \pm 0.105	0.662 \pm 0.101	0.845 \pm 0.029	0.817 \pm 0.050	0.765
SMOTE	0.700 \pm 0.046	0.639 \pm 0.069	0.689 \pm 0.059	0.730 \pm 0.052	0.690
Borderline-SMOTE	0.690 \pm 0.065	0.621 \pm 0.062	0.715 \pm 0.039	0.692 \pm 0.041	0.679
ADASYN	0.676 \pm 0.028	0.635 \pm 0.081	0.683 \pm 0.029	0.711 \pm 0.028	0.676
SVM-SMOTE	0.700 \pm 0.053	0.709 \pm 0.105	0.722 \pm 0.049	0.759 \pm 0.022	0.722
SMOTE-ENN	0.626 \pm 0.043	0.565 \pm 0.031	0.681 \pm 0.073	0.628 \pm 0.051	0.625
SMOTE-Tomek	0.684 \pm 0.020	0.659 \pm 0.058	0.674 \pm 0.060	0.693 \pm 0.043	0.677
TVAE	0.663 \pm 0.037	0.615 \pm 0.093	0.727 \pm 0.075	0.722 \pm 0.040	0.682
CTGAN	0.742 \pm 0.064	0.718 \pm 0.038	0.806 \pm 0.034	0.798 \pm 0.052	0.766
Gaussian Copula	0.762 \pm 0.033	0.738 \pm 0.042	0.754 \pm 0.060	0.805 \pm 0.065	0.765
Classifier avg.	0.698	0.656	0.730	0.735	—

The MLP column denotes the standardised feedforward baseline of Table A.7 (pytorch-tabular `CategoryEmbeddingModelConfig`, all features continuous) and is distinct from the prior-art deep networks of Khan et al. (DNN) and Reddy and Reddy (ANN), which are reproduced under their original configurations in Table A.12 (Appendix A.6). It is included as the canonical deep-tabular baseline against which the attention- and gating-based architectures (TabNet, FT-Transformer, GANDALF) are measured.

Table A.10: Per-class F1 (mean \pm std across 5 folds) for FT-Transformer under two configurations: seven-class no-aug and six-class no-aug. The hemiplegic row illustrates the effect of clinically motivated class aggregation: the merged class recovers $\approx +0.07$ F1 over the 7-class average of its two source subtypes (Sporadic 0.573, Familial 0.660 \rightarrow merged 0.691). Dashes denote classes that do not exist under that scheme.

Class	7-class (no aug)	6-class (no aug)
Migraine without aura	0.968 ± 0.029	0.967 ± 0.016
Typical aura with migraine	0.954 ± 0.010	0.957 ± 0.011
Typical aura without migraine	1.000 ± 0.000	1.000 ± 0.000
Basilar-type aura	0.843 ± 0.109	0.843 ± 0.109
Other	0.920 ± 0.098	0.920 ± 0.098
Sporadic hemiplegic migraine	0.573 ± 0.142	—
Familial hemiplegic migraine	0.660 ± 0.095	—
Hemiplegic migraine (merged)	—	0.691 ± 0.094
Macro-F1	0.845 ± 0.029	0.896 ± 0.038

Table A.11: Per-feature absolute mean differences between Sporadic ($n = 14$) and Familial ($n = 24$) Hemiplegic Migraine, sorted by $|\bar{x}_S - \bar{x}_F|$ ascending. DPF[†] is the only perfect separator (encoded as 0 for Sporadic and 1 for Familial). All remaining features are encoded as small non-negative integers in the public dataset.

Feature	\bar{x}_S	\bar{x}_F	$ \Delta $
Photophobia	1.000	1.000	0.000
Location	1.000	1.000	0.000
Character	1.000	1.000	0.000
Diplopia	0.000	0.000	0.000
Nausea	1.000	1.000	0.000
Hypoacusis	0.000	0.000	0.000
Phonophobia	1.000	1.000	0.000
Defect	0.000	0.000	0.000
Paresthesia	0.000	0.000	0.000
Tinnitus	0.286	0.292	0.006
Frequency	1.643	1.667	0.024
Vertigo	0.357	0.417	0.060
Dysarthria	0.071	0.000	0.071
Duration	1.500	1.583	0.083
Conscience	0.000	0.083	0.083
Age	21.571	21.458	0.113
Dysphasia	0.429	0.292	0.137
Vomit	0.429	0.208	0.220
Intensity	2.143	2.500	0.357
Sensory	0.571	0.208	0.363
Visual	1.786	1.333	0.452
DPF [†]	0.000	1.000	1.000

[†] DPF (*Direct Positive Family history*) is a binary indicator and the only feature that perfectly separates the two subtypes by construction; it does not provide discriminative structure for the underlying syndrome.

Table A.12: Leakage-free replication of the classifiers from the two prior studies: macro-F1 (mean \pm standard deviation, stratified 5-fold cross-validation, seven ICHD-3 classes) for every prior-art classifier reproduced under the leakage-free protocol, with no augmentation and with SMOTE fitted within each training fold. The best value per column is shown in bold. These figures are not comparable to the accuracy / CA values reported in the original studies, which were obtained with pre-split SMOTE (leakage).

Classifier	Source	No augmentation	SMOTE
SVM (linear, $C = 1$)	Khan + Reddy	0.784 ± 0.062	0.681 ± 0.040
KNN	Khan	0.710 ± 0.046	0.635 ± 0.075
Decision Tree	Khan	0.556 ± 0.066	0.610 ± 0.068
Random Forest (100 trees)	Khan	0.739 ± 0.096	0.729 ± 0.024
DNN	Khan	0.803 ± 0.077	0.702 ± 0.060
Logistic Regression	Reddy	0.785 ± 0.064	0.706 ± 0.028
Random Forest (10 trees)	Reddy	0.671 ± 0.082	0.700 ± 0.050
ANN	Reddy	0.801 ± 0.065	0.716 ± 0.038

The SVM (linear, $C = 1$) is common to both papers (Khan reports it explicitly; Reddy reports a linear kernel with C unreported, set to 1) and is computed once. Random Forest is reported by Khan (scikit-learn defaults, 100 trees) and by Reddy (a “minimal number of trees with growth control”, interpreted here as 10 trees), and is therefore listed separately by source. Settings reported by the authors were respected. The original studies reported accuracy between 88% and 99.7% (Khan) and CA between 0.958 and 0.995 (Reddy) under pre-split SMOTE (leakage); the macro-F1 values above are the corresponding leakage-free reevaluations.

References

- [1] L. J. Stovner, K. Hagen, M. Linde, T. J. Steiner, The global prevalence of headache: an update, with analysis of the influences of methodological factors on prevalence estimates, *J. Headache Pain* 23 (1) (2022) 34.
- [2] M. Ashina, Migraine, *The New England Journal of Medicine* 383 (19) (2021) 1866–1876. doi:10.1056/NEJMra1915327.
- [3] International Headache Society, The international classification of headache disorders, 3rd edition (ichd-3), *Cephalalgia* 38 (2018) 1–211. doi:10.1177/0333102417738202.
- [4] I. Petrušić, R. Messina, L. Pellesi, et al., Application of machine learning in migraine classification: a call for study design standardization and global collaboration, *The Journal of Headache and Pain* 26 (1) (2025) 200. doi:10.1186/s10194-025-02134-9.
- [5] W. Lee, M. K. Chu, The current role of artificial intelligence in the field of headache disorders, with a focus on migraine: A systemic review, *Headache and Pain Research* (Feb. 2025).
- [6] A. Stubberud, H. Langseth, P. Nachev, M. S. Matharu, E. Tronvik, Artificial intelligence and headache, *Cephalalgia* 44 (8) (2024) 3331024241268290.
- [7] G. S. Collins, K. G. M. Moons, P. Dhiman, R. D. Riley, A. L. Beam, B. Van Calster, M. Ghassemi, X. Liu, J. B. Reitsma, M. van Smeden, et al., TRIPOD+AI statement: updated guidance for reporting clinical prediction models that use regression or machine learning methods, *BMJ* 385 (2024) e078378. doi:10.1136/bmj-2023-078378.
- [8] L. Khan, M. Shahreen, A. Qazi, S. J. A. Shah, S. Hussain, H.-T. Chang, Migraine headache (MH) classification using machine learning methods with data augmentation, *Scientific Reports* 14 (1) (2024) 5180. doi:10.1038/s41598-024-55874-0.
- [9] A. Reddy, A. Reddy, Migraine triggers, phases, and classification using machine learning models, *Front. Neurol.* 16 (2025) 1555215.

- [10] H. He, E. A. Garcia, Learning from imbalanced data, *IEEE Transactions on Knowledge and Data Engineering* 21 (9) (2009) 1263–1284. doi: 10.1109/TKDE.2008.239.
- [11] D. M. Powers, Evaluation: From precision, recall and f-measure to roc, informedness, markedness and correlation, *Journal of Machine Learning Technologies* 2 (1) (2011) 37–63.
- [12] T. Saito, M. Rehmsmeier, The precision-recall plot is more informative than the ROC plot when evaluating binary classifiers on imbalanced datasets, *PLoS One* 10 (3) (2015) e0118432.
- [13] N. V. Chawla, K. W. Bowyer, L. O. Hall, W. P. Kegelmeyer, SMOTE: Synthetic minority over-sampling technique, *J. Artif. Intell. Res.* 16 (2002) 321–357.
- [14] R. Blagus, L. Lusa, SMOTE for high-dimensional class-imbalanced data, *BMC Bioinformatics* 14 (1) (2013) 106.
- [15] L. Xu, M. Skoularidou, A. Cuesta-Infante, K. Veeramachaneni, Modeling tabular data using conditional GAN, *CoRR* abs/1907.00503 (2019). arXiv:1907.00503.
URL <http://arxiv.org/abs/1907.00503>
- [16] S. Arik, T. Pfister, Tabnet: Attentive interpretable tabular learning, *Proceedings of the AAAI Conference on Artificial Intelligence* 35 (2021) 6679–6687.
- [17] G. Somepalli, M. Goldblum, A. Schwarzschild, M. Bruss, T. Goldstein, Saint: Improved neural networks for tabular data via row attention and contrastive pre-training, in: *Advances in Neural Information Processing Systems*, Vol. 34, 2021, pp. 23983–23994.
- [18] Y. Gorishniy, I. Rubachev, V. Khruikov, A. Babenko, Revisiting deep learning models for tabular data, in: *Advances in Neural Information Processing Systems*, Vol. 34, Curran Associates, Inc., 2021, pp. 18598–18608.
URL <https://proceedings.neurips.cc/paper/2021/hash/9d86d83f925f2149e9edb0ac3b49229c-Abstract.html>

- [19] N. Hollmann, S. Müller, K. Eggenberger, M. Lindauer, Tabular data: Deep learning is not all you need, *Advances in Neural Information Processing Systems* 35 (2022) 644–658.
- [20] V. Borisov, T. Leemann, K. Seßler, J. Haug, M. Pawelczyk, G. Kasneci, Deep neural networks and tabular data: A survey, *IEEE Transactions on Neural Networks and Learning Systems* 35 (2022) 7499–7519. doi:10.1109/TNNLS.2022.3229161.
- [21] L. Grinsztajn, E. Oyallon, G. Varoquaux, Why do tree-based models still outperform deep learning on tabular data?, *Advances in Neural Information Processing Systems* 35 (2022) 507–520.
- [22] R. Shwartz-Ziv, A. Armon, Tabular data: Deep learning is not all you need, *Information Fusion* 81 (2022) 84–90. doi:10.1016/j.inffus.2021.11.011.
- [23] I. Petrušić, A. Savić, K. Mitrović, N. Bačanin, G. Sebastianelli, D. Secci, G. Coppola, Machine learning classification meets migraine: recommendations for study evaluation, *The Journal of Headache and Pain* 25 (1) (2024) 215. doi:10.1186/s10194-024-01924-x.
- [24] C. Mosquera, L. Ferrer, D. H. Milone, D. Luna, E. Ferrante, Class imbalance on medical image classification: towards better evaluation practices for discrimination and calibration performance, *Eur. Radiol.* 34 (12) (2024) 7895–7903.
- [25] C. J. Hellín, A. A. Olmedo, A. Valledor, J. Gómez, M. López-Benítez, A. Tayebi, Unraveling the impact of class imbalance on deep-learning models for medical image classification, *Appl. Sci. (Basel)* 14 (8) (2024) 3419.
- [26] M. Sokolova, G. Lapalme, A systematic analysis of performance measures for classification tasks, *Information Processing & Management* 45 (4) (2009) 427–437. doi:10.1016/j.ipm.2009.03.002.
- [27] H. He, Y. Bai, E. A. Garcia, S. Li, ADASYN: Adaptive synthetic sampling approach for imbalanced learning, in: *2008 IEEE International Joint Conference on Neural Networks (IEEE World Congress on Computational Intelligence)*, IEEE, 2008, pp. 1322–1328.

- [28] H. Han, W.-Y. Wang, B.-H. Mao, Borderline-SMOTE: A new oversampling method in imbalanced data sets learning, in: *Lecture Notes in Computer Science, Lecture Notes in Computer Science*, Springer Berlin Heidelberg, Berlin, Heidelberg, 2005, pp. 878–887.
- [29] A. S. Tarawneh, A. B. Hassanat, G. A. Altarawneh, A. Almuhaimeed, Stop oversampling for class imbalance learning: A review, *IEEE Access* 10 (2022) 47643–47660.
- [30] N. Patki, R. Wedge, K. Veeramachaneni, The synthetic data vault, in: *2016 IEEE International Conference on Data Science and Advanced Analytics (DSAA)*, 2016, pp. 399–410. doi:10.1109/DSAA.2016.49.
- [31] J. Fonseca, F. Bacao, Tabular and latent space synthetic data generation: a literature review, *Journal of Big Data* 10 (1) (2023) 115. doi:10.1186/s40537-023-00792-7.
- [32] R. Sauber-Cole, T. M. Khoshgoftaar, The use of generative adversarial networks to alleviate class imbalance in tabular data: a survey, *Journal of Big Data* 9 (1) (2022) 98. doi:10.1186/s40537-022-00648-6.
- [33] S. Kapoor, A. Narayanan, Leakage and the reproducibility crisis in machine-learning-based science, *Patterns (N. Y.)* 4 (9) (2023) 100804.
- [34] D. Arp, E. Quiring, F. Pendlebury, A. Warnecke, F. Pierazzi, C. Wressnegger, L. Cavallaro, K. Rieck, Pitfalls in machine learning for computer security, *Commun. ACM* 67 (11) (2024) 104–112.
- [35] G. Lemaître, F. Nogueira, C. K. Aridas, Imbalanced-learn: A python toolbox to tackle the curse of imbalanced datasets in machine learning, *Journal of Machine Learning Research* 18 (17) (2017) 1–5.
- [36] M. Joseph, H. Raj, Gandalf: Gated adaptive network for deep automated learning of features (2024). arXiv:2207.08548, doi:10.48550/arXiv.2207.08548.
- [37] J. A. Sáez, J. Luengo, F. Herrera, Evaluating the classifier behavior with noisy data considering performance and robustness, *Information Sciences* 346–347 (2016) 256–274. doi:10.1016/j.ins.2016.03.050.

- [38] J. A. Sáez, J. Luengo, J. Stefanowski, F. Herrera, SMOTE-IPF: addressing the noisy and borderline examples problem in imbalanced classification by a re-sampling method with filtering, *Inf. Sci.* 291 (2015) 184–203. doi:10.1016/J.INS.2014.08.051.
URL <https://doi.org/10.1016/j.ins.2014.08.051>